AGU PUBLICATIONS

JGR

Journal of Geophysical Research: Atmospheres

RESEARCH ARTICLE
10.1002/2015JD023381

Key Points:
- Radiation, temperature, and water vapor relationships are explored
- CESM replicates many aspects of covariability among variables quite well
- CESM model rainfall and clouds undermine confidence in feedbacks

Correspondence to:
K. E. Trenberth,
trenbert@ucar.edu

Citation:
Trenberth, K. E., Y. Zhang, and J. T. Fasullo (2015), Relationships among top-of-atmosphere radiation and atmospheric state variables in observations and CESM, *J. Geophys. Res. Atmos.*, *120*, 10,074–10,090, doi:10.1002/2015JD023381.

Received 17 MAR 2015
Accepted 24 AUG 2015
Accepted article online 27 AUG 2015
Published online 9 OCT 2015

Relationships among top-of-atmosphere radiation and atmospheric state variables in observations and CESM

Kevin E. Trenberth[1], Yongxin Zhang[1], and John T. Fasullo[1]

[1]National Center for Atmospheric Research, Boulder, Colorado, USA

Abstract A detailed examination is made in both observations and the Community Earth System Model (CESM) of relationships among top-of-atmosphere radiation, water vapor, temperatures, and precipitation for 2000–2014 to assess the origins of radiative perturbations and climate feedbacks empirically. The 30-member large ensemble coupled runs are analyzed along with one run with specified sea surface temperatures for 1994 to 2005 (to avoid volcanic eruptions). The vertical structure of the CESM temperature profile tends to be top heavy in the model, with too much deep convection and not enough lower stratospheric cooling as part of the response to tropospheric heating. There is too much absorbed solar radiation (ASR) over the Southern Oceans and not enough in the tropics, and El Niño–Southern Oscillation (ENSO) is too large in amplitude in this version of the model. However, the covariability of monthly mean anomalies produces remarkably good replication of most of the observed relationships. There is a lot more high-frequency variability in radiative fluxes than in temperature, highlighting the role of clouds and transient weather systems in the radiation statistics. Over the Warm Pool in the tropical western Pacific and Indian Oceans, where nonlocal effects from the Walker circulation driven by the ENSO events are important, several related biases emerge: in response to high SST anomalies there is more precipitation, water vapor, and cloud and less ASR and outgoing longwave radiation in the model than observed. Different model global mean trends are evident, however, possibly hinting at too much positive cloud feedback in the model.

1. Introduction

Developing a predictive understanding of feedbacks in the climate system is critical for advancing knowledge of processes and their representation in climate models. The predominant human influence is through the changing composition of the atmosphere, especially through burning of fossil fuels and increasing greenhouse gases, thereby interfering with the ability of the planet to radiate heat to space. Yet this forced component of the energy imbalance is difficult to measure quite aside from the observational difficulties owing to the large natural variability associated with day-to-day weather that constitutes a form of climate noise. In this paper the focus is on the relatively high-frequency (monthly) relationships among a number of variables mainly within the atmosphere related to Earth's energy imbalance and how well they are simulated in the National Center for Atmospheric Research (NCAR) Community Earth System Model (CESM). However, we also have to deal with the trends that emerge even in the short 15 year period of the primary analysis.

At the top of atmosphere (TOA) observations from Clouds and the Earth's Radiant Energy System (CERES) [*Loeb et al*., 2009] have been used to examine the covariability with critical atmospheric variables that influence radiation. These data begin in March 2000, and that limits the time frame of this study. The net radiation at the TOA (R_T) consists of two components, the absorbed solar radiation (ASR) and the outgoing longwave radiation (OLR) such that $R_T = \mathrm{ASR} - \mathrm{OLR}$ is positive downward. *Trenberth et al*. [2015] have examined the mean and anomalies of these fields and their covariability with temperatures throughout the atmosphere, total column water vapor (Wv), and sea surface temperature (SST). Of particular interest in that study were not just the relationships among the global mean fields but also the spatial patterns of correlations and regression coefficients and thus how the local relationships cancel or reinforce each other to result in the global means. Using a model enables us to examine not only these fields but also model clouds, and we further add precipitation, both to serve as a proxy for cloud and convection and owing to their direct influence on surface temperature over land. The main updated observational results in *Trenberth et al.* [2015] are discussed when and as the model results are introduced.

The main model used here is CESM1. In *Trenberth et al.* [2014] we used the NCAR Community Climate System Model version 4 (CCSM4), but there have been major improvements in the cloud fields in CESM1 in which the atmospheric model changes from Community Atmosphere Model (CAM) CAM4 to CAM5 [*Kay et al*., 2012]. We also use the atmospheric model run with specified sea surface temperatures (SSTs) in so-called AMIP (Atmospheric Model Intercomparison Project) mode to enable examination of possible effects of biases in SSTs in the coupled model. Many of the relationships examined here in the model versus observations are remarkably good, but the discrepancies that exist are revealing, and we find that the diagnostics illustrated here are useful for evaluating model performance generally.

As shown in *Trenberth et al.* [2014, 2015], the variability in the Earth's energy imbalance is perhaps surprisingly large on monthly time scales. The standard deviations of monthly global mean anomalies of R_T are on the order of 0.65 W m^{-2}, and hence, fluctuations of ±1 W m^{-2} are common in the net downward radiation. Yet we seek small climate change signals associated with climate change of just a few tenths of a W m^{-2} over a decade. Most of the monthly variability has very short time scales and is associated with weather systems, such as the Madden-Julian Oscillation (MJO) in the tropics, or weather noise in the extratropics. Hence, some of the high-frequency variability is related to partial sampling of weather systems (part in one month and part in the next); at the surface, increased cloud reduces ASR and thus cools the surface, which in turn reduces OLR, and often the reverse happens the next month. Changes in cloud were inferred to play a major role, with temperatures typically acting as a strong negative feedback, while water vapor mostly amplifies temperature-related changes [*Trenberth et al*., 2015]. Only in the tropics, where warm subsiding air is also dry, are water vapor and temperatures not positively correlated. Given the mostly positive correlations between water vapor and temperature expected from the Clausius-Clapeyron relationship plus the negative correlations in tropical regions, it is of considerable interest to see whether models can replicate the structure and magnitude of these relationships. If it turns out that this is one aspect not done well in models, what are the implications for feedbacks, the energy imbalance, and climate sensitivity? It is these important questions we seek to illuminate in this paper.

2. Methods and Data Sets

The main sources of data are given in the Acknowledgments. At the TOA, observations from CERES begin in March 2000, constituting a nearly 15 year record (through October 2014 for this study), and have been used to examine the covariability with critical atmospheric variables that influence the radiation. We use the TOA shortwave, longwave, and net radiative fluxes, monthly on 1° × 1° grids, and "Energy Balanced and Filled" updated to version Ed2.8 [*Loeb et al*., 2009, 2012]. To the extent that the TOA solar irradiance is a function of season and latitude, anomalies in ASR are simply opposite to those in reflected shortwave radiation, although changes in irradiance such as with the 11 year solar cycle alter this.

The temperatures and water vapor come from analyzed fields from European Centre for Medium-Range Weather Forecasts-Interim (ERA-I) reanalysis [*Dee et al*., 2011]. Observed cloud fields were deemed too uncertain, and comparison with models too subjective, to be included. Surface air temperature and humidity trends over land in the ERA-I reanalysis compare well with observations [*Simmons et al*., 2010, 2014]. *Simmons et al.* [2014] demonstrate the excellent quality of ERA-I tropospheric temperatures, except that a change in source of SST data led to a shift to cooler SSTs by about 0.1 K in mid-2001 and thus lower tropospheric warming is somewhat underestimated. Also, there is some spurious variability in water vapor associated with changes in Special Sensor Microwave Imager data [*Trenberth et al*., 2011; *Trenberth and Fasullo*, 2013a], most notably a marked decrease starting in 1992. However, ERA-I did not include comprehensive TOA forcings and volcanic aerosols, such as those from the eruption of Mount Pinatubo in 1991. Accordingly, we have mostly confined diagnostics to the periods after March 2000, the CERES period.

Trenberth et al. [2015] examined the two meter air temperature (T_{2m}) and the temperature throughout the atmosphere (T_{all}), which was also divided up into the tropospheric temperature (T_{trop}), which is the vertical average below 150 hPa (about 13 km altitude), and the stratospheric temperature (T_{strat}), above 150 hPa. Wv was also considered, and the ERA-I reanalysis was used. We continue to use these variables here as well as precipitation. However, T_{trop} was defined as the mean temperature from 1000 to 150 hPa and therefore included a component extrapolated below the surface. To facilitate comparisons with the model, here we

use the surface to 150 hPa as the definition of T_{trop}. This makes very small changes in the values of correlations and regressions.

For precipitation, we use the monthly fields from the Global Precipitation Climatology Project, GPCP, data set on a 2.5° × 2.5° latitude/longitude grid that begins in 1979 [*Adler et al*., 2003]. Rain-gauge data, where available, are used to calibrate merged satellite-based rainfall estimates and to correct systematic bias [*Huffman et al*., 2009].

The Community Earth System Model Large Ensemble (CESM-LE) [*Kay et al*., 2015] consists of a 30-member set of runs using coupled atmosphere, ocean, land, and sea ice model components. The simulations span from 1920 to 2100 using estimated observed historical (through 2005) and Representative Concentration Pathway 8.5 projected external forcings from the Coupled Model Intercomparison Project 5 (CMIP5). For the analysis here, only simulated intervals spanning the recent historical record with an extension to the end of 2014 (2000–2014) are used in order to increase relevance to observed variability and avoid Pinatubo effects. The atmospheric component used is the CAM5.2 [*Hurrell et al*., 2013] run at 1.25° latitude-longitude resolution. Divergence in ensemble members is realized by imposing various small ($<10^{-12}$ K) perturbed initial conditions in the atmospheric temperature field in 1920 based on a single ensemble member beginning in 1850, which itself is initialized from an extended 1850 control run. For the purposes of this work, an important feature of CESM1(CAM5) is that it includes the aerosol indirect effects.

A single-member run of CAM5.3 using observed SSTs and a spectral element grid of approximately 1.3° effective resolution is used for CAM5-AMIP simulations for 1994 to 2005. SSTs are prescribed from observations from merged Hadley-Optimum Interpolation Sea Surface Temperature and sea ice concentration data sets [*Hurrell et al*., 2008]. Standard CMIP5 historical forcings are used including aerosols, solar irradiance, ozone, and greenhouse gases while observed SST and sea ice fraction are used at the surface. The start date is chosen to avoid effects of the Pinatubo eruption, and the runs available determine the finish date. As the period includes the large 1997–1998 El Niño event, it is of interest to see how robust the results are.

We have performed correlation and regression analyses of the temperatures, total column water vapor, precipitation, and cloud with OLR, ASR, and R_T. These have been performed locally but also as global means, and the differences between those results and the global mean of the local results can be substantial owing to cancellation, especially via effects of weather systems [*Trenberth et al*., 2015]. For CESM-LE and ERA-I results the period is 2000–2014, while for the observations involving CERES the period March 2000 to October 2014 is used. In these cases the two-sided 5% significance level is about 0.15 based on negligible observed monthly autocorrelations. The 30-member CESM-LE ensemble allows sampling issues to be addressed at least in the model context, and for this the 5% significance level for correlations is 0.03. Unfortunately, the observational period may not be very representative owing to the apparent hiatus in the rise of global mean surface temperatures [*Trenberth and Fasullo*, 2013b], and none of the model runs replicate the low observed trend (see Figure 4 presented later). Also, CESM model decadal variability may be underestimated [*Brown et al*., 2015].

As we shall see, for the model, there are significant trends in the ensemble mean, and accordingly, we have also computed correlations and regressions after removing the linear trend of the global mean. This was done to preserve the local relationships and remove only a very smoothed version of the ensemble mean that is undoubtedly forced. The variance of a series with a trend is

$$1/12{*}b^2 + s^2$$

where s is the standard deviation (SD) of the detrended series and b is the trend expressed as the change from the beginning to end in units of the variable. So for T_{2m}, the trend is on the order of 0.4 K over 15 years and $b = 0.4$. The first term is then 0.0133. If $s = 1$ then the variance is 1.013 or the SD is 1.007, i.e., a 0.7% increase. In fact, s is much larger than this everywhere over land and less than 0.5 only over some parts of the ocean. Even if the trend is 0.5, and $s = 0.5$, then the variance increase is still only 4%. Hence, it is not surprising that trends contribute negligibly to the local correlations and the full result is therefore presented. Only for the global mean fields does the trend make a difference and these are discussed.

3. Temporal Variations and Temperature Relationships

The dominant interannual variations in TOA radiative fluxes in the tropics occur with El Niño–Southern Oscillation (ENSO), which involves a buildup of heat during La Niña and a discharge of heat during El Niño

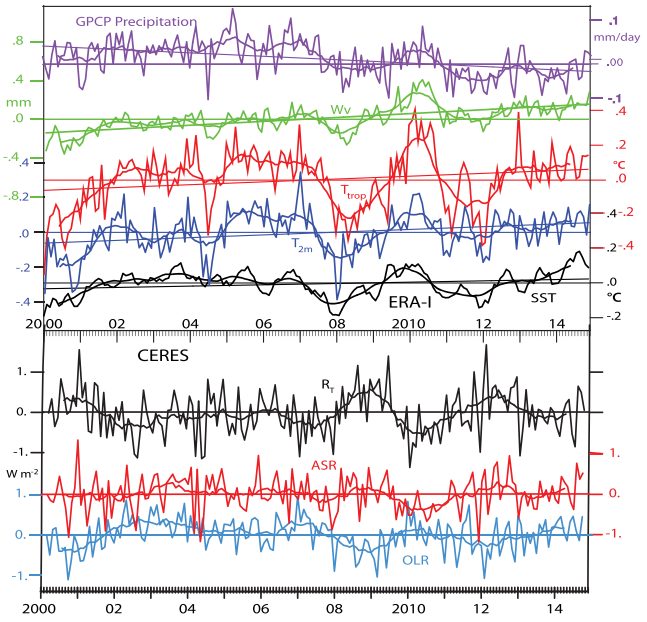

Figure 1. Observed monthly anomalies for 2000–2014 in global mean precipitation in mm d^{-1}; total column water vapor (Wv) in mm; T_{trop}, T_{2m}, and SST in K; and R_T, ASR, and OLR in W m^{-2}. The thin straight line is the linear trend, and a 12 month running mean is also included.

[*Trenberth et al.*, 2002a, 2002b, 2014]. The SST anomalies during El Niño events are sustained by ocean heat transports that allow the events to persist for a year or so. However, there is considerable month-to-month variability associated with weather fluctuations: storms of all sorts in the extratropics and the MJO in the tropics. For 2000 to 2014, the observed time series (Figure 1) show no significant trend for R_T, ASR, and OLR and only small upward trends for SST, T_{2m}, T_{trop}, and Wv while the small trend in precipitation is negative. The interannual variability is dominated by ENSO and has a presence in all variables, but there is also clearly a lot of superposed monthly noise. For 1994–2005 for the observations and the AMIP runs, a dominant feature is the 1997–1998 El Niño event (not shown).

To understand the forcing of the CESM-LE runs, Figure 2 presents the TOA incoming solar radiation, which exhibits a sunspot cycle that is realistic but smoothed. It differs very slightly from the observed Solar Radiation and Climate Experiment (SORCE) value [*Kopp*, 2014]. *Vernier et al.* [2011] describe the contributions of aerosols to forcings in the 2000s, but these are missing in the CMIP5 models including CESM. Contributions of small volcanoes contribute order 0.1 W m^{-2} negative forcing [*Trenberth et al.*, 2014]. The main forcings are the steadily increasing greenhouse gases that were prescribed from observations. The net effect of all forcings can be best summarized by examining the global mean ocean heat content (OHC) (Figure 2) which shows the effects of the volcanic eruptions El Chichón in 1982 and Pinatubo in 1991 but the otherwise steady increase in heating of the planet over the period of our analysis. The increase in OHC from the early 1980s to 2010 on the order of 2×10^{23} J is similar to estimates of the observed value [*Balmaseda et al.*, 2013].

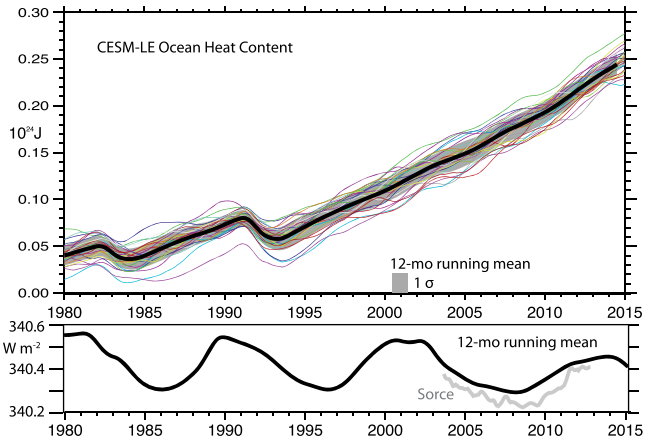

Figure 2. (top) The 12 month running mean changes in total ocean heat content for the individual runs as well as the ensemble mean ± 1 standard deviation (shaded in gray) as an indicator of the total forcing of the system in 10^{24} J. (bottom) For CESM-LE, the 12 month running mean of the TOA solar irradiance along with observed values from SORCE is shown.

A commonly used index for representing SST variability associated with ENSO is the Oceanic Niño Index of NOAA (ONI), an area average of monthly SST anomalies in the region 5°N–5°S, 170°–120°W, referred to as the Niño3.4 region. Time series of the ONI from all members of the ensemble (not shown) reveal that there are large ENSO fluctuations; in fact, they are too large in amplitude by about 44%, as was also the case for CCSM4 [*Deser et al.*, 2012]. The model standard deviation for ONI is 1.086°C versus observed 0.75°C (1900–2011 [*Deser et al.*, 2012]).

The overall trends are best revealed in the 30-member ensemble global means (Figure 3). Linear trends are indicated for all model variables in Figure 3. The

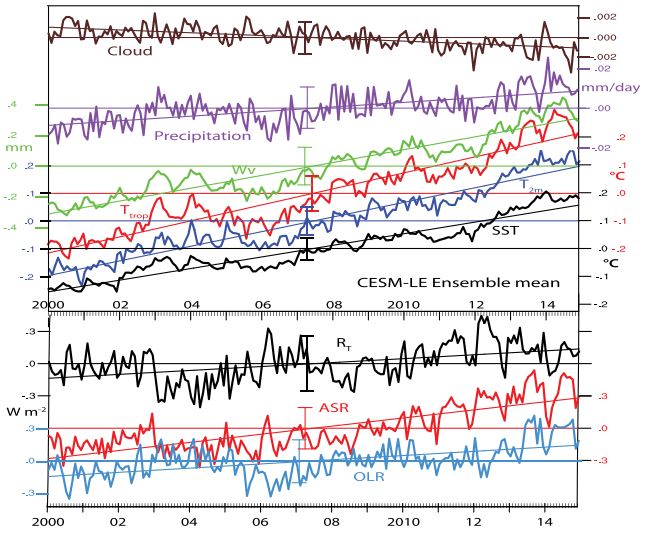

Figure 3. Ensemble means of several fields averaged over the 30 runs for 2000–2014 monthly anomalies for total cloud fraction; precipitation in mm d^{-1}; Wv in mm; T_{trop}, T_{2m}, and SST in K; and R_T, ASR, and OLR in W m^{-2}. The standard error σ_E about the ensemble mean is plotted near the center of the time series as $0 \pm 2\sigma_E$. The linear trend line is also plotted.

global mean SST increases over the 15 years by about 0.3°C, T_{2m} by 0.4°C, and T_{trop} by 0.4°C, all larger than observed. Precipitation and total column water vapor Wv also increase, by about 0.02 mm d^{-1} and 0.6 mm, respectively, while cloud fraction decreases by 0.2%. The net increase in heating is seen in R_T, which increases by 0.3 W m^{-2} over the 15 years. However, the main source of that heating is the increase in ASR (0.6 W m^{-2}) while OLR contributes to planetary cooling by 0.3 W m^{-2}. This perhaps surprising result, given that the forcing is increased trapping of longwave radiation by greenhouse gases, is actually common in models [*Trenberth and Fasullo*, 2009] and will be explored more later.

The entire set of global T_{2m} time series (Figure 4) concatenated has a monthly standard deviation of 0.18°C, and after detrending each member the value is 0.14°C compared with the ERA-I values of 0.16°C for both (Figure 4). The linear trends are also shown (Figure 4), and the observed value (0.12°C) is lower than any of the 30 ensemble members and roughly half the lowest model ensemble member trend. This relates to the apparent hiatus in observed global warming [*Trenberth and Fasullo*, 2013b]. However, the ERA-I trend is possibly underestimated owing to multiple sources of SST used [*Dee et al.*, 2011]. Changes occurred in mid-2001 as well as January 2002 and 2009. Alternative estimates of global mean temperatures have 2014 as the warmest year on record, but this is not the case for ERA-I.

Figure 5 presents global mean temperatures from four members of CESM-LE as height time series of anomalies. Figure 5c presents the member with the largest surface trend; Figure 5d presents the one with the smallest, and the others are randomly chosen. A similar plot for the observations for 1979 to 2013 was given in *Trenberth et al.* [2015]. The El Niño events show up as tropospheric warmings in the global mean temperatures (Figure 5) but with corresponding coolings in the stratosphere above 100 hPa. However, the stratospheric coolings are nowhere near as distinct in the model results.

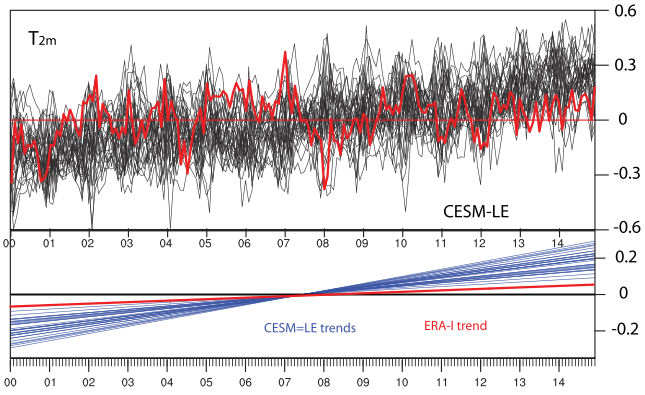

Figure 4. All 30 ensemble members of CESM-LE are presented for monthly global mean anomalies of T_{2m} along with an observational estimate from ERA-I in red. (bottom) The linear trend from each series is given.

To characterize the vertical structure we have performed empirical orthogonal function analysis of all the model runs and the observations, but the result is perhaps best seen by simply correlating global mean values at all levels with the 300 hPa value (Figure 6). We can do this also individually for each of the 30 ensemble members and thereby form a standard error of the mean, which is plotted at several levels. As well as the full time series at each level we also use the global detrended values (dashed lines). The observed value for 1979–1993 is also plotted (dotted) to bring out the different stratospheric results when major volcanic eruptions

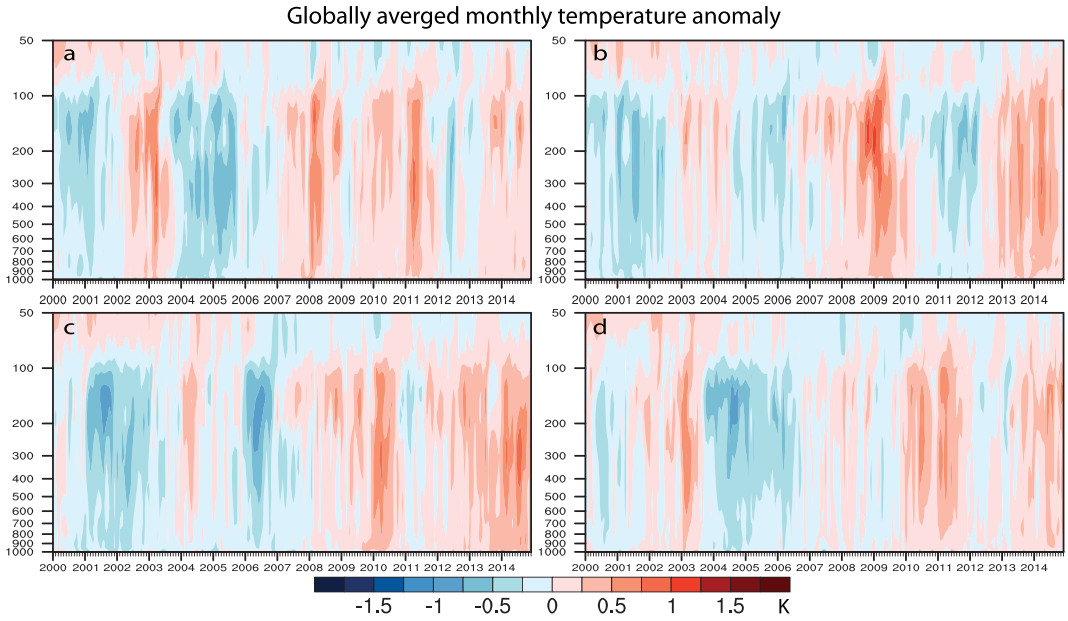

Figure 5. Four ensemble members of global mean temperature monthly anomaly time series (K). (c) The member with the largest T_{2m} trend and (d) the smallest.

are present. The model correlations at the surface are slightly stronger than the observations, but the main differences are above 300 hPa where the model result is "top heavy" with too much penetration of the tropospheric signal into the lower stratosphere. Cooling trends are strong in the model in the stratosphere going along with warming in the troposphere, but the detrended values suggest that the fluctuations above 50 hPa have the same sign and are much bigger than observed. Hence, the reversal in sign observed in the lower stratosphere 30–70 hPa is not as strong in the model as observed. It is likely that the former relates to excessive simulated deep convection in the tropics. It is also evident in the AMIP run with specified SSTs and thus is not primarily a result of ocean coupling.

Santer et al. [2008] examined the vertical profile of temperature in the tropics for models versus observations. However, we find that the vertical profile is rather different when volcanic eruptions are included than when they are excluded (Figure 6). In particular, the observed stratospheric warming with both El Chichón and Pinatubo greatly influenced the tropopause height [*Santer et al.*, 2003] and penetrated down to 200 hPa [*Trenberth et al.*, 2015], while this is not the case in the model (not shown). Hence, the modeling of volcanic eruption responses can be a source of discrepancy in this regard, and this also influences the so-called satellite temperature records of *Santer et al.* [2008]. Ozone changes also affect stratospheric temperature trends.

4. Spatial Structure

4.1. Mean Fields

Documentation of only a few of the mean fields is given here for these model runs as we prefer to focus on the covariability of certain fields. Characteristics of the model precipitation are revealed in comparisons of the annual mean and the seasonal differences (Figure 7). The AMIP results (not shown) are very similar to those for the CESM-LE. The annual mean model bias shows excess precipitation over the oceans but deficits in Southeast Asia and the Amazon region, both strong monsoon regions. By focusing on the December-January-February (DJF)-June-July-August (JJA) differences in precipitation, we can reveal aspects of the large forced response to the annual cycle. In observations (Figure 7), the opposite signs north and south of about the equator reveal both surpluses in summer monsoonal rains and deficits in storm track regions, where precipitation is greatest in winter. On land at high latitudes, cold temperatures in winter diminish water availability, and hence, rainfall is greater in summer. The model results reveal slightly stronger seasonal changes, consistent with a more vigorous hydrological cycle overall. Throughout the tropics over the oceans,

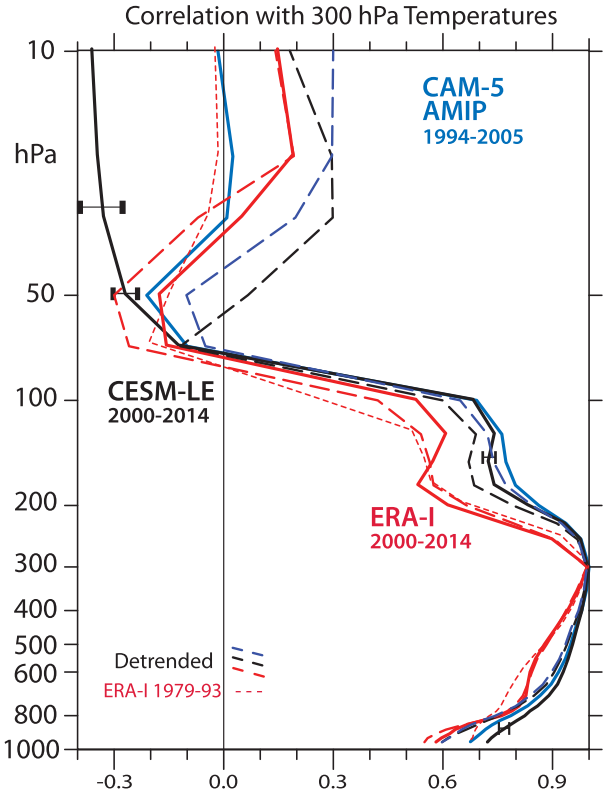

Figure 6. Correlations of monthly mean anomalies of global mean temperatures at each level with that at 300 hPa for ERA-I (red) for 2000–2014, CAM5 AMIP (blue) for 1994–2005, and CESM-LE (black) for 2000–2014. On the latter ±2 standard error bars are included at several levels. Also given are the results for the detrended time series as dashed lines. The red dotted profile is for ERA-I for 1979–1993 to show effects of two major volcanic eruptions.

especially the Pacific, the errors relate to the chronic problem of the double Intertropical Convergence Zone (ITCZ) structure and the tendency for the ITCZ to be too strong in the southern hemisphere.

The performance of the model in terms of TOA radiation (Figure 8) shows that the annual mean net radiation R_T biases are dominated by those in ASR: too much absorbed solar radiation over the southern hemisphere extratropical oceans and too little ASR over the tropics including the tropical continents, consistent with the "too few too bright" bias in tropical clouds [*Nam et al.*, 2012]. Accordingly, these biases are strongest in the summer and relate mostly to clouds and their optical thickness. As a result there is considerable compensation between ASR and OLR throughout the tropics. High bright clouds not only reflect radiation, reducing ASR, but also emit less to space from the cold cloud tops, reducing OLR [*Kiehl*, 1994]. Problems in ASR over the Southern Oceans [*Gettelman et al.*, 2012; *Kay et al.*, 2014] are long-standing [*Trenberth and Fasullo*, 2010] and relate to cloud liquid water in low-level and midlevel clouds on the cold side of cyclonic circulations [*Bodas-Salcedo et al.*, 2014].

4.2. Local Correlations

Because we are interested in global mean values, and how they come about, the main analysis in this section is about the local relationships. However, we first examine how the local values of temperature relate to the global mean for the observations and CESM-LE for T_{2m} and T_{trop} (Figure 9) [cf. *Brown et al.*, 2015]. The global T_{2m} value is correlated with the monthly mean T_{2m} values in fairly similar ways for the model and observations (detrending makes little difference). Individual monthly anomalies, not the ensemble mean, are used for the model. Both feature a strong ENSO pattern component, although the CESM-LE is much stronger in the eastern Pacific, consistent with the too strong ENSO variations in the model. The global mean of the local correlations is also greater for the model. The time series for global mean T_{trop} differ somewhat from T_{2m} (Figures 1 and 3), and the right plots show that the local correlations feature a fairly zonally symmetric pattern that, while different from the left plots, also arises from ENSO [*Trenberth and Smith*, 2006, 2009]. Again, the values are somewhat stronger in the model.

The local correlations between T_{2m} and precipitation (Figure 10) reveal predominantly negative values over land, except for Antarctica, in both observations and model runs. This relates very much to water availability issues [*Trenberth and Shea*, 2005], whereby cyclonic conditions favor cloudy skies, rain, and high soil moisture, and thus less sensible heat and greater latent heat components of the surface fluxes, resulting in lower temperatures accompanying rain. In contrast, in anticyclonic conditions, relatively clear skies and more sunshine mean more incoming energy at the surface, less rain, drier soils, more sensible heating and less evaporation, and thus higher temperatures with less rain. These circumstances are unique to land because water availability for evapotranspiration is never an issue over the ocean.

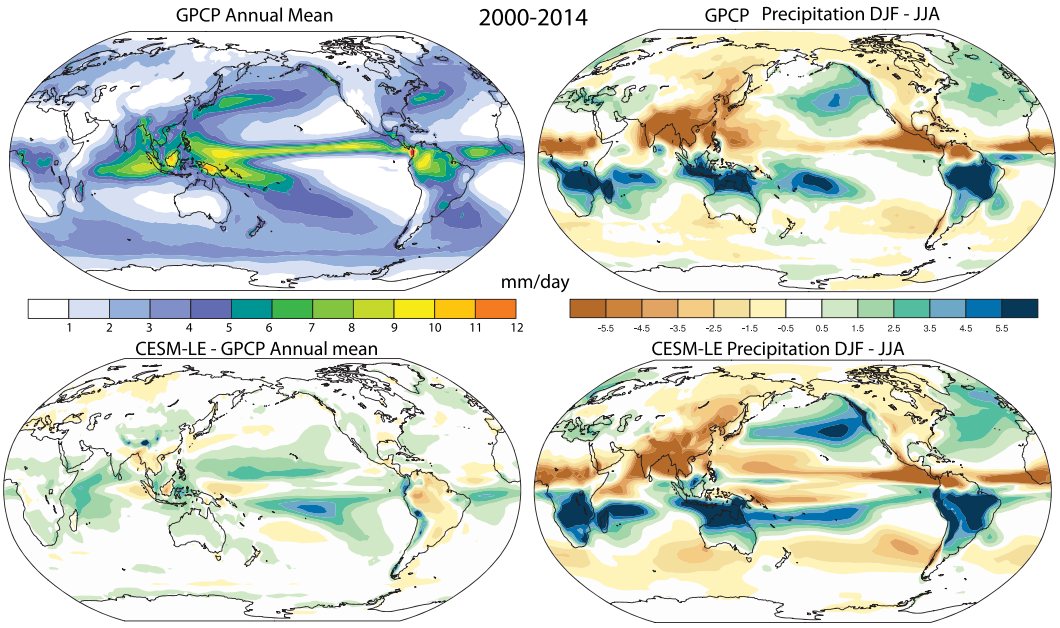

Figure 7. (top left) Observed (GPCP) annual mean precipitation and (top right) difference between DJF and JJA in mm d^{-1} for 2000–2014. Difference from the top plot for the (bottom left) CESM-LE runs and (bottom right) CESM-LE DJF-JJA. The color bar at middle right applies to the top right and bottom plots.

In addition, in the observations there is a large area of negative correlations over the western tropical Pacific-Indonesian-tropical Indian Ocean regions. In contrast, the model results reveal mostly positive correlations over the ocean, especially where El Niño results in higher SSTs. This has been a long-standing characteristic of models [*Hurrell and Trenberth*, 1999]. Further examination of this relationship shows that teleconnections with ENSO are important; in particular, the strong Walker circulation reversal with El Niño results in subsidence over the western Pacific region that overrides any relationship with local SSTs. The model fails to accurately reproduce this influence, either in AMIP runs (Figure 10b) or in fully coupled mode (Figure 10c). This region is also noted for where the supergreenhouse effect occurs [*Soden and Fu*, 1995; *Bony et al*., 1997; *Inamdar et al*., 2004]. Note also that the correlations between global mean values are much more positive than the mean of the global values, signifying the larger variance and dominance of the ENSO effects, and more so in the model than observed.

The relationships between temperatures and water vapor are also revealing (Figure 11). Strongest positive correlations $>$0.7 occur in the extratropics poleward of about 40° latitude, but the regression values are small because the total amounts of water vapor are so low compared with the tropics. In the tropics, high precipitation, cloud, and water vapor go hand-in-hand and imply lower surface temperatures through reduced ASR and evaporative cooling effects on land. In the extratropics, warm and moist advection go together in baroclinic weather systems, and the Clausius-Clapeyron relationship of warm air holding more moisture plays a strong role to give strong positive correlations, that dominate globally. The Wv -T_{trop} relationships differ somewhat but clearly call out the tropical-subtropical atmospheric dynamics associated with the main convergence zones and subsidence regions [*Soden and Fu*, 1995; *Bony et al*., 1997]. In the convergence zones where upward motion prevails, large cloud amount, Wv, and precipitation are associated with latent heat release, a moist adiabatic lapse rate and higher temperatures above the surface, while in subsidence regions the warming of the desiccated sinking air at the dry adiabatic lapse rate makes for high temperatures with less Wv. In the coupled model, positive correlations are more widespread than observed, especially in the southeast Pacific for T_{trop} and in the Warm Pool region of the western tropical Pacific-Indian Ocean region for T_{2m}. In the southeast Pacific this problem likely relates to the huge errors in the mean ASR field and cloud cover (Figure 8). Negative correlations between T_{2m} and Wv occur where they are also observed to be negative with precipitation (Figure 10). Interestingly, the AMIP run recovers some of this structure, although it is still deficient for T_{2m}. This suggests that biases arising from atmosphere-ocean coupling are part of the issue here, and the model has stronger correlations between global mean Wv and T_{2m} and T_{trop} than observed, as a result.

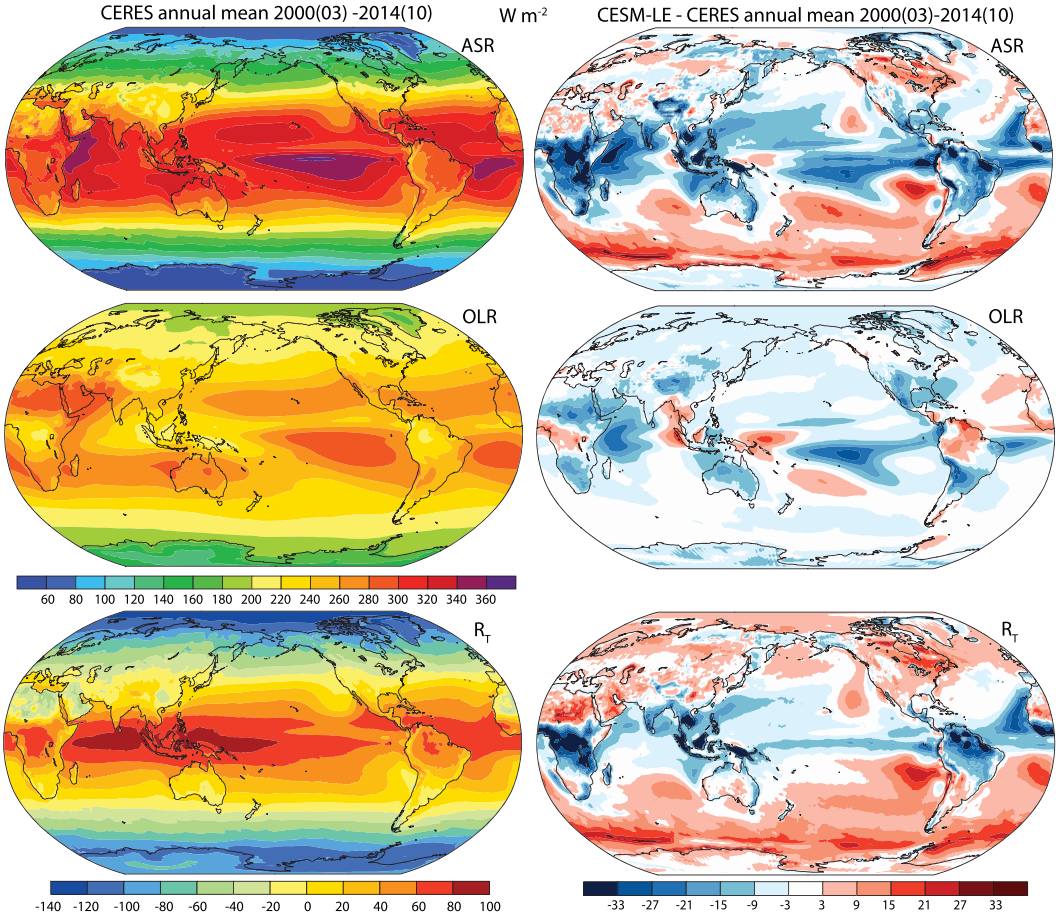

Figure 8. (left) Radiation at TOA in W m^{-2} from CERES for March 2000 to October 2014 and (right) differences for the CESM-LE for (top) ASR, (middle) OLR, and (bottom) R_T.

The correlations of monthly mean anomalies of T_{2m} and T_{trop} with ASR and OLR (Figures 12 and 13) have some similarities, especially for T_{2m}, and reveal considerable structure. For ASR the result is very similar but opposite in sign for the model results to correlations of the temperatures with total cloud cover (not shown), except in very high latitudes, where sea ice and land ice play a role [*Hartmann and Ceppi*, 2014]. In general, the model results replicate the observations quite well.

For T_{2m} with ASR, the relationship is predominately positive, as higher ASR (i.e., less cloud) leads to higher surface temperatures except in the deep tropical Pacific where high SSTs cause deep convection, high cold clouds, and less ASR. Also, where snow and ice play a role, higher temperatures imply lower surface albedo and more ASR. The T_{2m} with OLR relationship is also largely positive as higher temperatures radiate more to space, except for the deep tropics where high cold cloud tops radiate less to space above high SSTs.

For OLR the positive land signature emerges strongly and is well replicated by the model. This is especially the case for relationships between OLR and T_{trop}. However, ASR with T_{trop} differs considerably from the T_{2m} relationship. The high positive correlations in mountain areas suggest a role for snow cover: higher temperatures imply less snow, and thus more ASR, while more ASR also implies higher temperatures as a snow-feedback effect. But over oceans the relationships are mainly negative, indicating that cloud responses to SST play a major role, and higher temperatures in warm advection in extratropical storms are accompanied by more cloud and less ASR.

In general, these observed spatial patterns are quite well reproduced by the model. This is especially true over land. However, over the ocean, there are marked differences in the tropical western Pacific and Indian Oceans where observed positive correlations of ASR with T_{2m} are largely negative in both coupled and AMIP configurations. The same is true for OLR; the positive correlations observed with T_{2m} are mostly

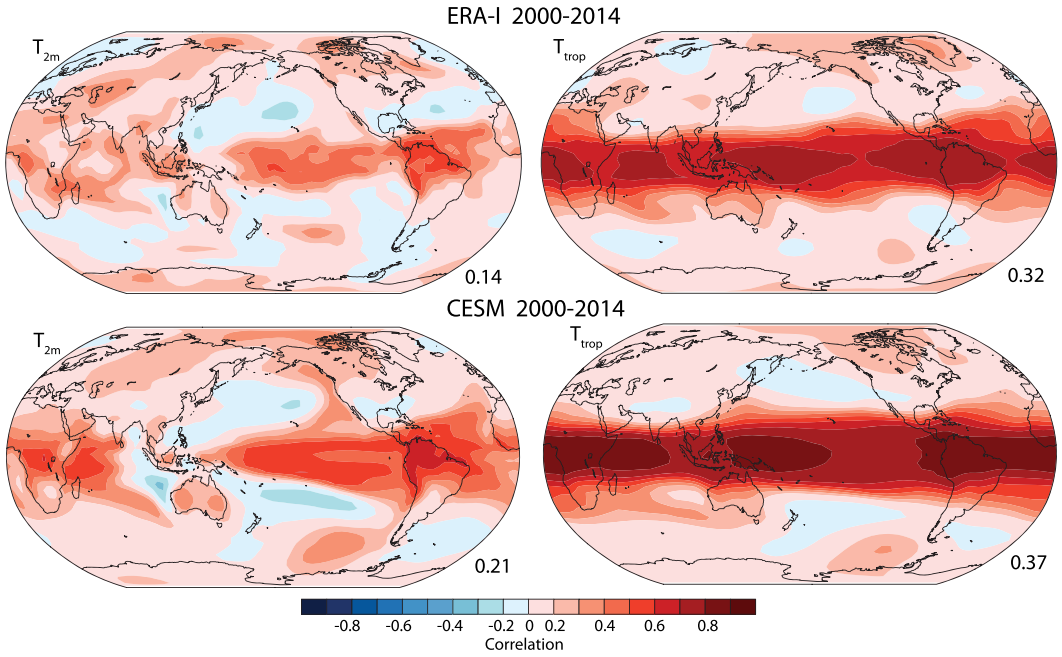

Figure 9. Correlations of individual monthly mean anomalies between global values and local values of (left) T_{2m} and (right) T_{trop} for 2000–2014 for observations from (top) ERA-I and (bottom) CESM-LE. At bottom right the global mean correlation is given for each.

negative in the model. As a result, there is large cancellation of error in R_T. The area identified here where the problems occur is similar to that for precipitation discrepancies and is physically related (Figure 10). Important differences occur in the correlations of the global mean values, and these are of most importance for overall system behavior.

Observed correlations between global means for ASR-T_{2m} are 0.16 versus about 0.35 in the model and for T_{trop} −0.2 versus about 0.1 in the model. For OLR, the correlations are also higher: for T_{2m} 0.45 observed versus 0.51 and 0.54 for AMIP and CESM-LE, respectively, and 0.55 versus 0.71 and 0.67 for T_{trop}. The global mean of the ASR correlations versus the correlations between the global means is higher because the ocean relationship dominates, while the reverse is true for OLR indicating the important role of the land in the global mean in radiating to space. However, maps of correlations of global mean temperature with local values (Figure 9) bring out the coherence of the tropics [cf. *Trenberth and Smith*, 2006, 2009], and ENSO relationships prevail in the observations. This is also true for the AMIP run but not for CESM-LE where global warming plays a stronger role in determining the global mean result (discussed further below).

There is a large cancellation between ASR and OLR, and it is not obvious from Figures 12 and 13 what the net result for R_T should be (Figure 14). This cancellation applies for many clouds but especially the high cold clouds in the deep tropics. The corresponding regression maps (not shown) factor in the variance of the fields and are more meaningful when the global means are computed, and it is evident that the tropics are the region where these relationships dominate global variance. However, the global means of the regression and correlation coefficients (Figure 14) are positive with T_{2m} but strongly negative for T_{trop}. In general, the pattern and magnitude of the local correlations in Figure 14 are quite similar between the model and observations. The biggest differences are in the tropical eastern Pacific associated with ENSO, especially for the AMIP run which includes the big 1997–1998 El Niño event. Yet the two model results for different periods and couplings are remarkably similar.

4.3. Global Relationships

It is apparent that often the global mean relationships do not apply locally, where day-to-day weather and cloud variations may dominate. Further, the global mean relationships may not have much relationship to those between means of the global values where regional variance differences also come into play. Table 1 summarizes regression results for global mean fields. To examine sampling uncertainties, all regression coefficients

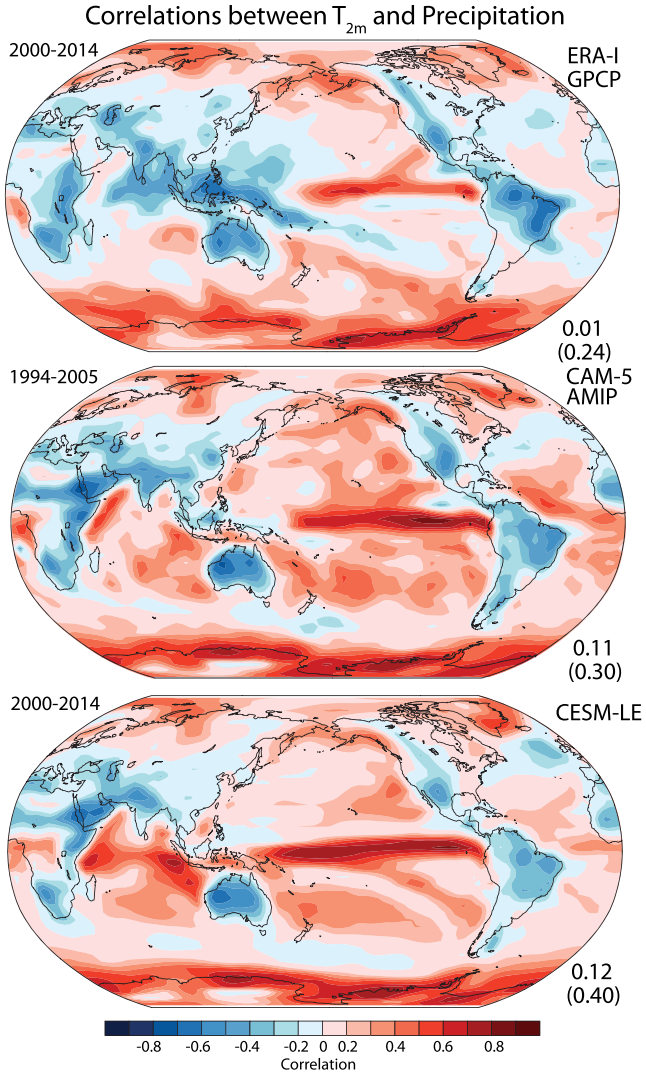

Figure 10. Local correlation coefficients between T_{2m} and precipitation amount for (top) observations 2000–2014, (middle) CAM5-AMIP for 1994–2005, and (bottom) CESM-LE for 2000–2014 monthly anomalies. At bottom right of each plot the global mean of the local correlations is given as well as, in parentheses, the correlation between the global mean values.

were computed for every CESM-LE ensemble member, and standard deviations computed, as well as rankings established. The 2nd and 29th out of 30 values are shown to indicate the 6.7 to 93.3% range.

The observed value between global means of T_{2m} with R_T of $-1.00\,W\,m^{-2}K^{-1}$ is less than the two model results (-0.87 and -0.64, respectively) although within sampling expectations. However, the observed T_{trop} value $-2.18\,W\,m^{-2}K^{-1}$ is significantly more negative than for the coupled model. The OLR regression is low, but the ASR value more than compensates and is highly significantly different from observed, signaling model problems with clouds.

However, these results for the CESM-LE are influenced by the trends evident in Figure 3 that are largely absent in the observations. From Table 1, it can be seen how the R_T regression values arise and the effects of trends. For the observations, the effect is small. For the model though, the detrended OLR relationship is much stronger. The trend in temperature leads to a fourth power increased contribution to OLR. The global correlation drops from 0.73 detrended to 0.67 between OLR and T_{trop}. However, the strong positive trend in ASR is mostly responsible for the surface and tropospheric warming, and the positive relationship between the linear trends increases the ASR and R_T correlations and regressions that are otherwise dominated by ENSO. With the ASR relationship more negative when detrended, the regression with R_T becomes much stronger in the model than observed.

The values in Table 1 may be relevant to the climate feedback parameter [*Dessler*, 2013]. For T_{2m}, the negative R_T regression is dominated by the strong OLR radiation to space as temperatures increase while the ASR anomaly is distinctly positive. The latter arises as excess incoming radiation heats the surface, and this is stronger in the model than the observations (cf. Figure 8). However, for T_{trop}, for the observations the ASR regression coefficient is significantly negative unlike the models. These results depend on clouds. Higher temperatures generally increase OLR but clouds offset this, and those clouds also reduce ASR, much more in observations than in the models. For the total field, the net result is a stronger radiative damping for temperatures in the observations than implied by the model versions. So a question is whether this result further implies smaller climate sensitivity?

The main cause of the model warming is an increase in absorbed solar radiation (Figure 3), as was true in most CMIP3 models [*Trenberth and Fasullo*, 2009]. To understand the trends and their influences better, we explored the trend maps and local maps (not shown). By far the biggest warming at the surface in CESM-LE occurs in the

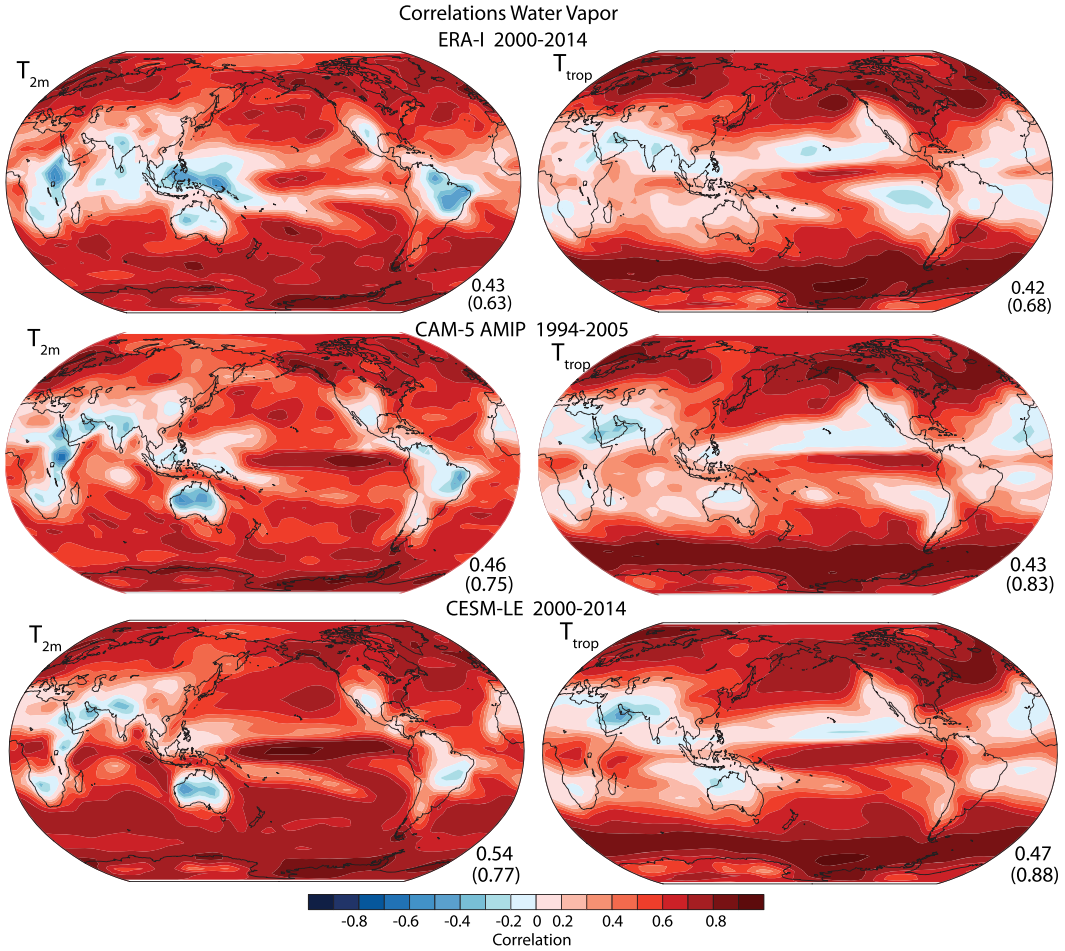

Figure 11. Local correlation coefficients between (left) T_{2m}-Wv and (right) T_{trop}-Wv for (top) observations 2000–2014, (middle) CAM5-AMIP for 1994–2005, and (bottom) CESM-LE for 2000–2014 monthly anomalies. At bottom right of each plot the global mean of the local correlations is given as well as, in parentheses, the correlation between the global mean values.

Arctic, and this is not out of line with the observed trends there. However, they are also strongly positive around Antarctica, which is not observed at all. Ice-albedo effects clearly come into play, as the main increases in ASR occur for clear sky and in summer. These effects extend over land to as far south as 40°N, and from 60–70°S, much more than observed for this period.

However, there are also substantial decreases in total cloud amount in the model, from 30–90°N and 10–50°S (see also Figure 3), although in the Arctic this is mainly in the winter where it does not influence ASR, although it does affect OLR. It is likely that these responses are erroneous and arise especially because of the biases in the clouds and radiation (Figure 8). This version of CESM has too strong effects from so-called indirect effects of aerosols on clouds that have been greatly improved very recently [*Gettelman et al.*, 2015]. Hence, the result depends on the scenario used for aerosols, which is not realistic. Accordingly, there are good reasons not to trust the trends and question the model implications for feedback and climate sensitivity.

5. Concluding Remarks

Making use of the available CERES data, we examine the relationships among TOA radiation and water vapor and temperatures in the atmosphere from ERA-I in an effort to assess the origins of radiative perturbations and climate feedbacks empirically and compared with CESM model results. The covariability of monthly mean anomalies in the CESM runs, both in fully coupled mode and for AMIP runs, where the surface SSTs are specified, produces remarkably good replication of most of the observed relationships examined here.

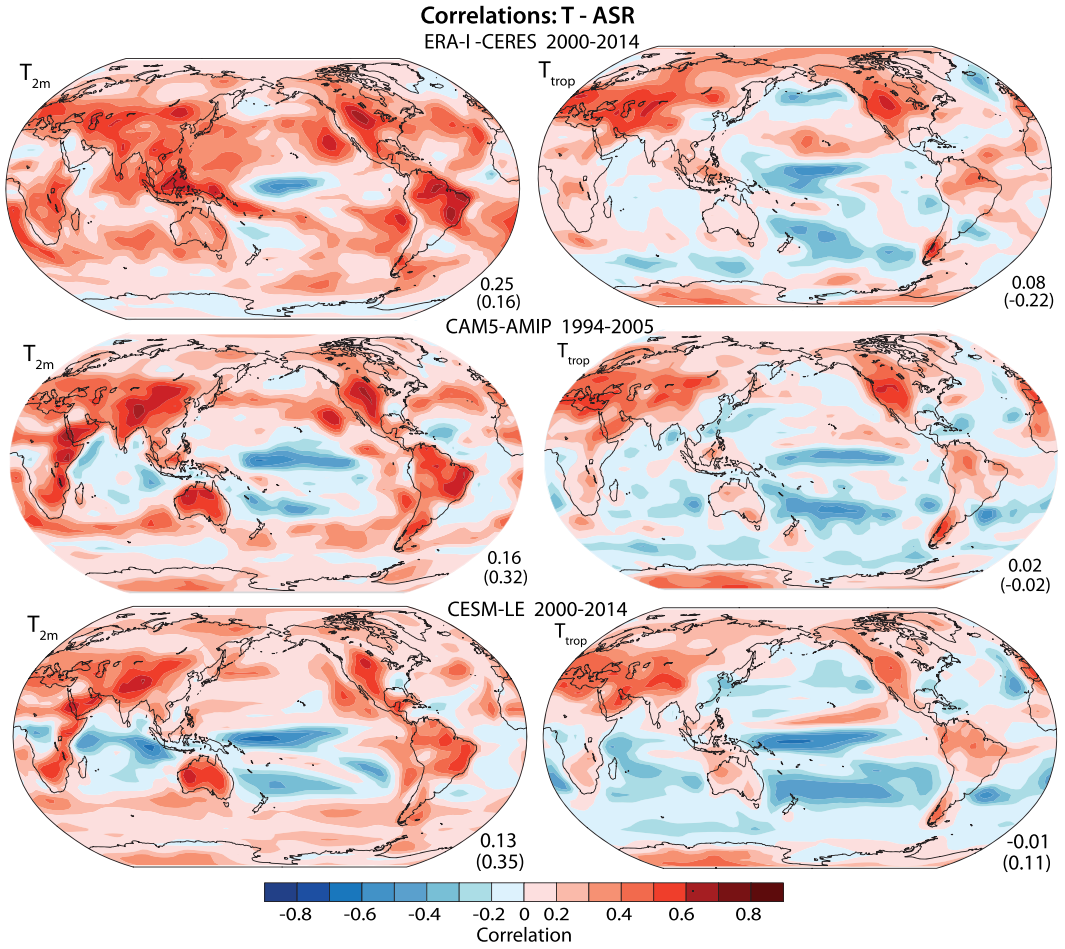

Figure 12. Local correlation coefficients between monthly anomalies of (left) T_{2m}-ASR and (right) T_{trop}-ASR for (top) observations (March 2000 to October 2014), (middle) CAM5-AMIP for 1994–2005, and (bottom) CESM-LE for 2000–2014. At bottom right of each plot the global mean of local correlations is given as well as, in parentheses, the correlation between the global mean values.

The observed period is quite short (15 years), and the model forcings are not realistic, although their variability is fairly small.

Increases in cloud amount and precipitation decrease ASR and reduce surface temperature. Over the ocean, the latter occurs in SST but is small, while much larger responses occur over land, not only in surface temperatures but also in surface moisture and evapotranspiration that also play a role. Otherwise, in most of the physical relationships, the implied causality is that the changes in temperature, water vapor, and cloud, while perhaps arising themselves from remote effects of the dynamics, affect the radiation, rather than the radiation causing changes in the local temperature. There is a lot more high-frequency variability in radiative fluxes than there is in temperature, highlighting the role of clouds and transient weather systems in the radiation statistics. The strongest relationship overall is that increased temperatures lead to more OLR. In particular, land areas, especially in the extratropics, provide a strong window for radiation to escape to space that is well replicated in the model. The biggest exception is in the deep tropics where high SSTs are accompanied by deep convection and high cold cloud tops, and thus less ASR and OLR, and while these effects mostly cancel for R_T there are some differences in the model result.

Although there is good qualitative agreement between the model and observations, the comparisons reveal some outstanding issues. The ENSO in the model is supersized and is some 40% or so larger than observed, which is an issue with this model. This may itself relate to biases in the sensitivities explored here in addition to other (e.g., ocean) processes. Major biases exist in the ASR, in particular, with too much ASR over the

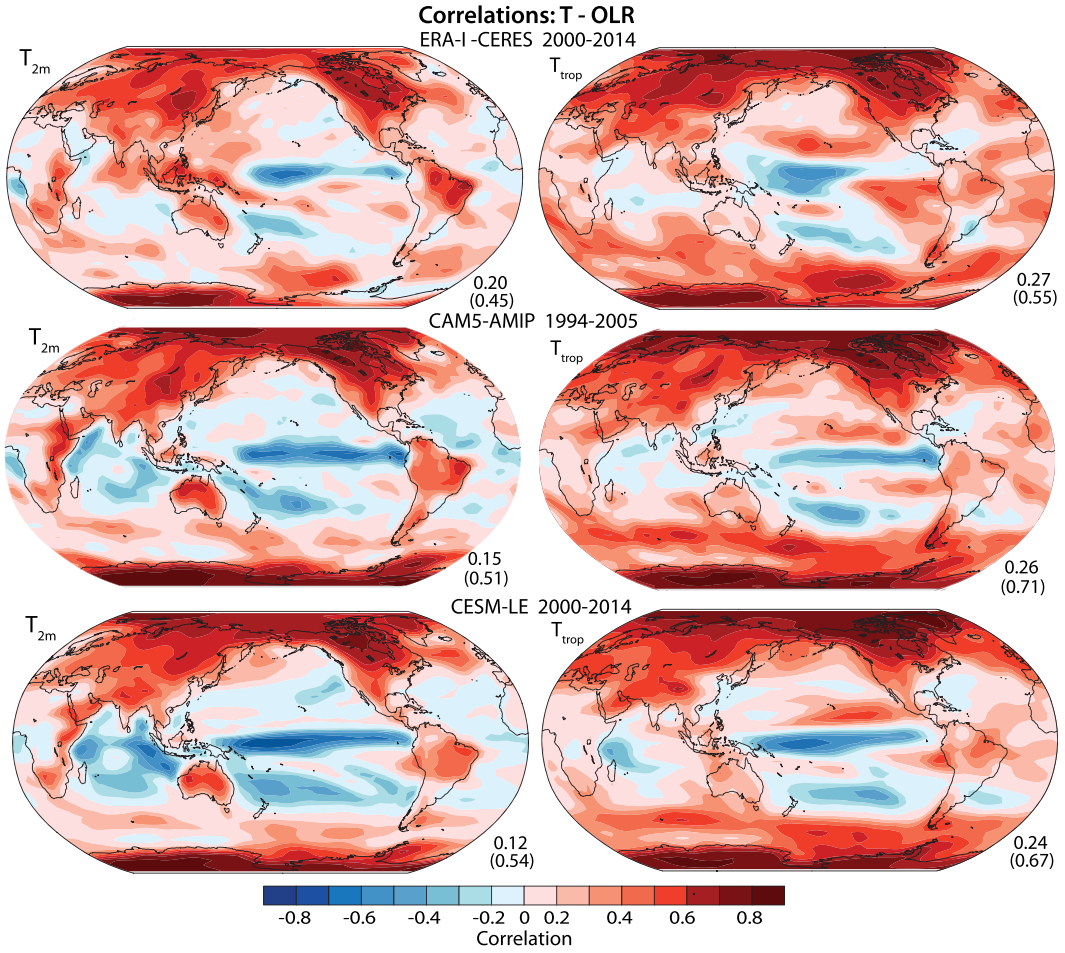

Figure 13. Local correlation coefficients between monthly anomalies of (left) T_{2m}-OLR and (right) T_{trop}-OLR for (top) observations (March 2000 to October 2014), (middle) CAM5-AMIP for 1994–2005, and (bottom) CESM-LE for 2000–2014. At bottom right of each plot the global mean of local correlations is given as well as, in parentheses, the correlation between the global mean values.

Southern Oceans and not enough in the tropics, so that this also biases meridional gradients and alters ocean heat transports. The ASR biases are echoed in R_T. Nor can disagreement with observations be dismissed as merely arising from internal variability. Moreover, as has been seen here, the global values depend critically on cancellation of effects both regionally (involving teleconnections) and among variables (such as ASR versus OLR) that may not offset unless all of the processes are well replicated. Of particular concern is the existence of a double ITCZ bias in models.

The vertical structure of the temperature profile is shown to be top heavy in the model, with too much deep convection and not enough lower stratospheric cooling as part of the Rossby wave response to heating. This profile may be very useful as a standard test for parameterized convection schemes under development. There are also signs that the relationship between water vapor and temperatures in subsiding air in the tropics is a critical test that some models do not do well. It has been shown to be important in discriminating among the climate sensitivity of models [*Fasullo and Trenberth*, 2012].

Most of the monthly variability has very short time scales and is associated with weather systems. The biggest discrepancies revealed in the local correlation maps are most clearly over the tropical western Pacific and Indian Oceans Warm Pool. Over the oceans, where nonlocal effects from the Walker circulation driven by the ENSO events in the central and eastern Pacific play a key role, several related biases emerge. When SST anomalies are high there is more precipitation over the oceans in the model both in coupled and AMIP modes that is not observed in the Warm Pool region (Figure 10). There is more water vapor (Figure 11)

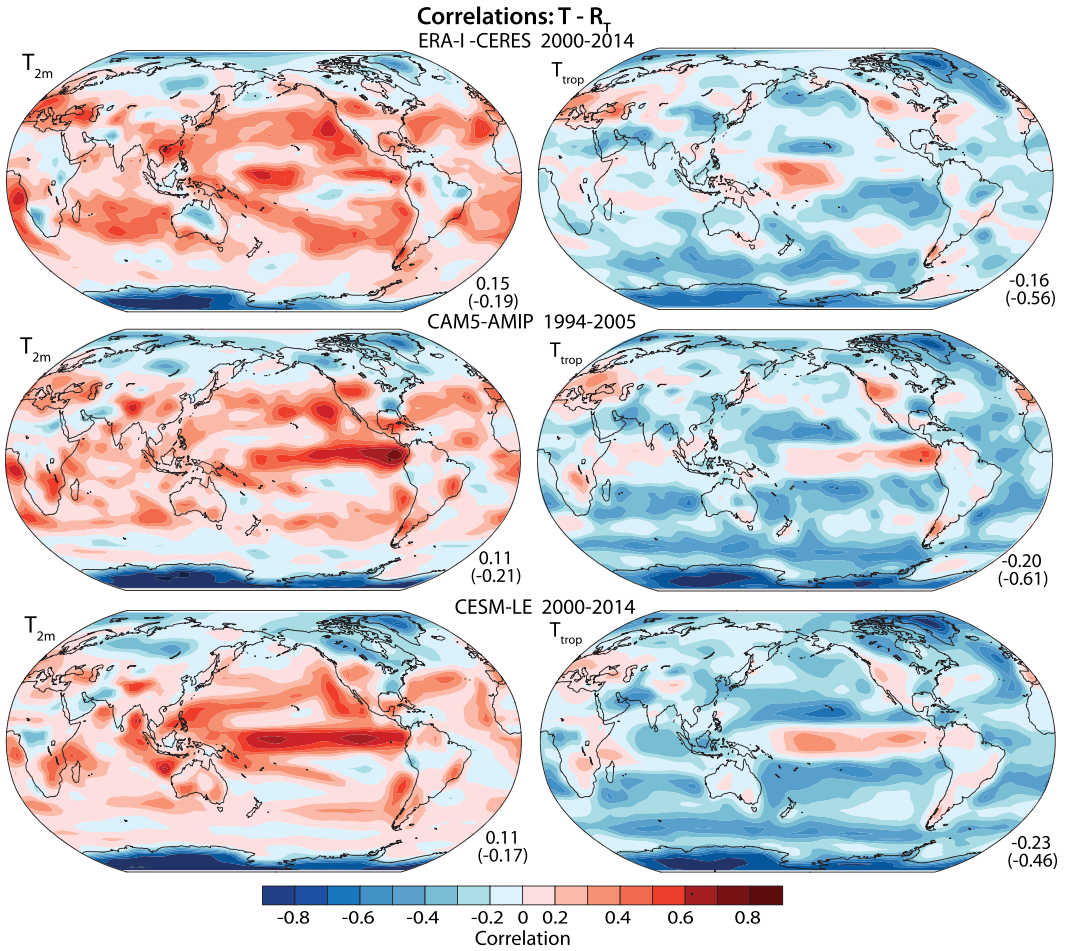

Figure 14. Local correlation coefficients between monthly anomalies of (left) R_T-T_{2m} and (right) R_T-T_{trop} for (top) observations (March 2000 to October 2014), (middle) CAM5-AMIP for 1994–2005, and (bottom) CESM-LE for 2000–2014. At bottom right of each plot the global mean is given as well as, in parentheses, the correlation between the global mean values.

and cloud (Figure 12) under these circumstances, and as a result, both ASR and OLR (Figure 13) are smaller in the model than in the real world. These biases have potential implications both for climate sensitivity and canonical model biases such as the cold-tongue bias because they modulate lateral heating gradients. In CESM-LE R_T is also too small around and south of India (Figure 8), although this bias in R_T is not evident in

Table 1. Regression Coefficients Between T_{2m} and T_{trop} With R_T, ASR, and OLR for the Observed 2000(03)–2014(10), CAM5-AMIP 1994–2005, and CESM-LE 2000–2014 Models in W m^{-2} K^{-1}[a]

	T_{2m}			T_{trop}		
	R_T	ASR	OLR	R_T	ASR	OLR
Observed	−1.00	0.66	1.66	**−2.18**	**−0.66**	1.52
CAM5-AMIP	−0.87	0.92	1.78	−1.97	−0.05	1.91
CESM-LE	−0.64	1.04	1.68	−1.45	0.26	1.72
Spread	−1.4; −0.1	0.7; 1.5	1.4; 2.0	−1.9; −0.9	−0.1; 0.7	1.5; 1.9
Detrended	R_T	ASR	OLR	R_T	ASR	OLR
Observed	−1.12	0.70	**1.81**	−2.26	**−0.68**	**1.58**
CESM-LE	−1.55	0.77	2.32	−2.61	−0.31	2.30
Spread	−1.9; −0.8	0.4; 1.2	1.9; 2.8	−3.1; −2.2	−0.6; 0.1	2.1; 2.5

[a]For CESM-LE, regressions were computed for each of 30 members and the 2nd and 29th values are given to indicate the 6.7 and 93.3 percentiles: labeled "spread." Note that R_T = ASR − OLR. The lowest two rows provide regression results after detrending each set. The bold observed values are significantly different to those from CESM-LE.

the AMIP run. However, the variances of temperatures in this region are relatively small compared with especially those on land, and hence, they do not contribute a lot to the global mean regressions.

The correlation between global monthly mean surface temperature and net radiation anomalies over the March 2000 to October 2014 period is only −0.19 and is very similar in the model runs. There is a lot more confidence in the stronger relationship with tropospheric temperature. Vertically averaged tropospheric temperatures correlate significantly with net incoming radiation at −0.56 globally, with a regression coefficient of $-2.18 \pm 0.10\,\mathrm{W\,m^{-2}\,K^{-1}}$. The latter is somewhat lower in the model runs here, and it relates to the biases in ASR and thus cloud, but it also changes by 80% in the model when the results are detrended. It is difficult to say whether this is simply because of the anomalous period used, particularly as the observed global mean surface temperature in the 2000s failed to increase substantially [*Trenberth and Fasullo*, 2013b]. Nevertheless, the kind of analysis performed here provides considerable insights into covariability among various variables that relate strongly to feedback processes important in gauging response to forcings and natural variability. It seems possible that model development and climate sensitivity estimates could be refined using these methods, given the strong regional structures and the extent to which they compensate and the need to go well beyond global means and surface temperatures.

Acknowledgments

This research is partially sponsored by NASA under grant NNX11AG69G and DOE grant DE-SC0012711. The data sets are discussed in section 2, and those used are public domain and available for CERES from Langley Atmospheric Science Data Center (http://ceres.larc.nasa.gov/order_data.php), ERA-I (http://data-portal.ecmwf.int/data/d/interim_-daily/), and GPCP (ftp://precip.gsfc.nasa.gov/pub/gpcp-v2.2/). The CESM-LE output data are publicly available via the Earth System Grid (https://www.earthsystemgrid.org). NCAR is sponsored by the National Science Foundation.

References

Adler, R. F., et al. (2003), The version 2 Global Precipitation Climatology Project (GPCP) monthly precipitation analysis (1979-present), *J. Hydrometeorol.*, *4*(6), 1147–1167.

Balmaseda, M. A., K. E. Trenberth, and E. Källén (2013), Distinctive climate signals in reanalysis of global ocean heat content, *Geophys. Res Lett.*, *40*, 1–6, doi:10.1002/grl.50382.

Bodas-Salcedo, A., K. D. Williams, M. A. Ringer, I. Beau, J. N. S. Cole, J.-L. Dufresne, T. Koshiro, B. Stevens, Z. Wang, and T. Yokohata (2014), Origins of the solar radiation biases over the Southern Ocean in CFMIP2 models, *J. Clim.*, *27*, 41–56, doi:10.1175/JCLI-D-13-00169.1.

Bony, S., K.-M. Lau, and Y. C. Sud (1997), Sea surface temperature and large-scale circulation influences on tropical greenhouse effect and cloud radiative forcing, *J. Clim.*, *10*, 2055–2077, doi:10.1175/1520-0442(1997)010<2055:SSTALS>2.0.CO;2.

Brown, P. T., W. Li, and S.-P. Xie (2015), Regions of significant influence on unforced global mean surface air temperature variability in climate models, *J. Geophys. Res. Atmos.*, *120*, 480–494, doi:10.1002/2014JD022576.

Dee, D. P., et al. (2011), The ERA-Interim reanalysis: Configuration and performance of the data assimilation system, *Q. J. R. Meteorol. Soc.*, *137*, 553–597.

Deser, C., et al. (2012), ENSO and Pacific decadal variability in Community Climate System Model version 4, *J. Clim.*, *25*, 2622–2651, doi:10.1175/JCLI-D-11-00301.1.

Dessler, A. E. (2013), Observations of climate feedbacks over 2000–10 and comparisons to climate models, *J. Clim.*, *26*, 333–342, doi:10.1175/JCLI-D-11-00640.1.

Fasullo, J. T., and K. E. Trenberth (2012), A less cloudy future: The role of subtropical subsidence in climate sensitivity, *Science*, *338*, 792–794, doi:10.1126/science.1227465.

Gettelman, A., J. E. Kay, and K. M. Shell (2012), The evolution of climate sensitivity and climate feedbacks in the community atmosphere model, *J. Clim.*, *25*, 1453–1469, doi:10.1175/JCLI-D-11-00197.1.

Gettelman, A., H. Morrison, S. Santos, and P. Bogenschutz (2015), Advanced two-moment bulk microphysics for global models. Part II: Global model solutions and aerosol–cloud interactions, *J. Clim.*, *28*, 1288–1307, doi:10.1175/JCLI-D-14-00103.1.

Hartmann, D. L., and P. Ceppi (2014), Trends in the CERES dataset, 2000–13: The effects of sea ice and jet shifts and comparison to climate models, *J. Clim.*, *27*, 2444–2456, doi:10.1175/JCLI-D-13-00411.1.

Hurrell, J. W., and K. E. Trenberth (1999), Global sea surface temperature analyses: Multiple problems and their implications for climate analysis, modeling and reanalysis, *Bull. Am. Meteorol. Soc.*, *80*, 2661–2678.

Hurrell, J. W., J. J. Hack, D. Shea, J. M. Caron, and J. Rosinski (2008), A new sea surface temperature and sea ice boundary dataset for the Community Atmosphere Model, *J. Clim.*, *21*, 5145–5153.

Hurrell, J. W., et al. (2013), The Community Earth System Model: A framework for collaborative research, *Bull. Am. Meteorol. Soc.*, *94*, 1339–1360, doi:10.1175/BAMS-D-12-00121.1.

Huffman, G. J., R. F. Adler, D. T. Bolvin, and G. Gu (2009), Improving the global precipitation record: GPCP version 2.1, *Geophys. Res. Lett.*, *36*, L17808, doi:10.1029/2009GL040000.

Inamdar, A. K., V. Ramanathan, and N. G. Loeb (2004), Satellite observations of the water vapor greenhouse effect and column longwave cooling rates: Relative roles of the continuum and vibration-rotation to pure rotation bands, *J. Geophys. Res.*, *109*, D06104, doi:10.1029/2003JD003980.

Kay, J. E., et al. (2012), Exposing global cloud biases in the Community Atmosphere Model (CAM) using satellite observations and their corresponding instrument simulators, *J. Clim.*, *25*, 5190–5207.

Kay, J. E., B. Medeiros, Y.-T. Hwang, A. Gettelman, J. Perket, and M. G. Flanner (2014), Processes controlling Southern Ocean shortwave climate feedbacks in CESM, *Geophys. Res. Lett.*, *41*, 616–622, doi:10.1002/2013GL058315.

Kay, J. E., et al. (2015), The Community Earth System Model (CESM) Large Ensemble Project: A community resource for studying climate change in the presence of climate variability, *Bull. Am. Meteorol. Soc.*, *96*, doi:10.1175/BAMS-D-13-00255.1.

Kiehl, J. (1994), On the observed near cancellation between longwave and shortwave cloud forcing in tropical regions, *J. Clim.*, *7*, 559–565.

Kopp, G. (2014), An assessment of the solar irradiance record for climate studies, *J. Space Weather Space Clim.*, *4*, A14, doi:10.1051/swsc/2014012.

Loeb, N. G., B. A. Wielicki, D. R. Doelling, G. L. Smith, D. F. Keyes, S. Kato, N. Manalo-Smith, and T. Wong (2009), Toward optimal closure of the Earth's top-of-atmosphere radiation budget, *J. Clim.*, *22*, 748–766.

Loeb, N. G., J. M. Lyman, G. C. Johnson, R. P. Allan, D. R. Doelling, T. Wong, B. J. Soden, and G. L. Stephens (2012), Observed changes in top-of-the-atmosphere radiation and upper ocean heating consistent within uncertainty, *Nat. Geosci.*, *5*, 110–113, doi:10.1038/NGEO1375.

Nam, C., S. Bony, J.-L. Dufresne, and H. Chepfer (2012), The "too few, too bright" tropical low-cloud problem in CMIP5 models, *Geophys. Res. Lett.*, *39*, L21801, doi:10.1029/2012GL053421.

Santer, B. D., et al. (2003), Contributions of anthropogenic and natural forcing to recent tropopause height changes, *Science*, *301*, 479–483.

Santer, B. D., et al. (2008), Consistency of modelled and observed temperature trends in the tropical troposphere, *Int. J. Climatol.*, *28*, 1703–1722, doi:10.1002/joc.1756.

Simmons, A. J., K. M. Willett, P. D. Jones, P. W. Thorne, and D. P. Dee (2010), Low-frequency variations in surface atmospheric humidity, temperature, and precipitation: Inferences from reanalyses and monthly gridded observational data sets, *J. Geophys. Res.*, *115*, D01110, doi:10.1029/2009JD012442.

Simmons, A. J., P. Poli, D. P. Dee, P. Berrisford, H. Hersbach, S. Kobayashib, and C. Peubey (2014), Estimating low-frequency variability and trends in atmospheric temperature using ERA-Interim, *Q. J. R. Meteorol. Soc.*, *140*, 329–353, doi:10.1002/qj.2317.

Soden, B. J., and R. Fu (1995), A satellite analysis of deep convection, upper-tropospheric humidity, and the greenhouse effect, *J. Clim.*, *8*, 2333–2351, doi:10.1175/1520-0442(1995)008<2333:ASAODC>2.0.CO;2.

Trenberth, K. E., and J. T. Fasullo (2009), Global warming due to increasing absorbed solar radiation, *Geophys. Res. Lett.*, *36*, L07706, doi:10.1029/2009GL037527.

Trenberth, K. E., and J. T. Fasullo (2010), Simulation of present day and 21st century energy budgets of the Southern Oceans, *J. Clim.*, *23*, 440–454.

Trenberth, K. E., and J. T. Fasullo (2013a), Regional energy and water cycles: Transports from ocean to land, *J. Clim.*, *26*, 7837–7851, doi:10.1175/JCLI-D-00008.1.

Trenberth, K. E., and J. T. Fasullo (2013b), An apparent hiatus in global warming?, *Earth's Future*, *1*, 19–32, doi:10.1002/2013EF000165.

Trenberth, K. E., and D. J. Shea (2005), Relationships between precipitation and surface temperature, *Geophys. Res. Lett.*, *32*, L14703, doi:10.1029/2005GL022760.

Trenberth, K. E., and L. Smith (2006), The vertical structure of temperature in the tropics: Different flavors of El Niño, *J. Clim.*, *19*, 4956–4973.

Trenberth, K. E., and L. Smith (2009), Variations in the three dimensional structure of the atmospheric circulation with different flavors of El Niño, *J. Clim.*, *22*, 2978–2991, doi:10.1175/2008JCLI2691.1.

Trenberth, K. E., D. P. Stepaniak, and J. M. Caron (2002a), Interannual variations in the atmospheric heat budget, *J. Geophys. Res.*, *107*(D8), 4066, doi:10.1029/2000JD000297.

Trenberth, K. E., J. M. Caron, D. P. Stepaniak, and S. Worley (2002b), Evolution of El Niño–Southern Oscillation and global atmospheric surface temperatures, *J. Geophys. Res.*, *107*(D8), 4065, doi:10.1029/2000JD000298.

Trenberth, K. E., J. T. Fasullo, and J. Mackaro (2011), Atmospheric moisture transports from ocean to land and global energy flows in reanalyses, *J. Clim.*, *24*, 4907–4924, doi:10.1175/2011JCLI4171.1.

Trenberth, K. E., J. T. Fasullo, and M. A. Balmaseda (2014), Earth's energy imbalance, *J. Clim.*, *27*, 3129–3144, doi:10.1175/JCLI-D-13-00294.

Trenberth, K. E., Y. Zhang, J. T. Fasullo, and S. Taguchi (2015), Climate variability and relationships between top-of-atmosphere radiation and temperatures on Earth, *J. Geophys. Res. Atmos.*, *120*, 3642–3659, doi:10.1002/2014JD022887.

Vernier, J.-P., et al. (2011), Major influence of tropical volcanic eruptions on the stratospheric aerosol layer during the last decade, *Geophys. Res. Lett.*, *38*, L12807, doi:10.1029/2011GL047563.